Morphologies of AB Diblock Copolymer Melts Confined in Nanocylindrical Tubes

Jie Feng and Eli Ruckenstein*

Department of Chemical and Biological Engineering, State University of New York at Buffalo, Buffalo, New York 14260-4200

Received March 16, 2006; Revised Manuscript Received May 2, 2006

ABSTRACT: Monte Carlo simulations have been employed to identify the morphologies of symmetrical AB diblock copolymer melts under the confinement of nanocylindrical tubes. The effects of (i) the incommensurability between the diameter of the tube and the lamellae period in the bulk and (ii) the preference of the tube surface for one of the segments have been investigated. Lamellae normal to the tube axis and circular lamellae have been observed under the conditions investigated, in agreement with experiment and density functional calculations. Furthermore, porous lamellar (mesh) morphologies, lamellae parallel to the tube axis as well as single and double helixes have been identified.

I. Introduction

The phase behavior of diblock copolymer melts has been considered an important topic by theorists and experimentalists due to the rich microstructures and interesting applications in the nanotechnology and biological areas.[1,2] The initial investigations were concerned with bulk block copolymer melts. Spheres and cylinders as well as lamellae and bicontinuous gyroid structures have been identified both experimentally and theoretically.[3,4] However, these microscale ordered structures change their orientation in various parts of the system, and at macroscale, the structure may no longer look ordered. It is also well-known that the structure of the self-assembly of polymers is strongly affected by external fields, which can break the symmetry of the morphologies present when the field is absent, generating more ordered morphologies. To achieve ordered periodical structures, surface, shear as well as electrical fields have been employed.[5−22]

Lamellae normal to the surfaces have been observed in symmetrical AB diblock copolymer melts confined between neutral or weakly selective parallel walls.[6−8] When the interaction between the wall and blocks became stronger and the melted films were sufficiently thin, the orientation of the lamellae was determined by the commensurability between the film thickness and the characteristic period L_0 of the lamellae in the bulk melt.[8] For film thicknesses nL_0 for symmetrical walls and $(n + {}^1/_2)L_0$ for asymmetrical ones, where n is an integer, lamellae parallel to the surfaces were observed. In contrast, when n was an integer $+ {}^1/_2$, the parallel lamellae were replaced by normal ones. When very strong selective walls and sufficiently thick but not too thick copolymer melt films were employed, parallel lamellae were formed.[8]

He et al.[23] investigated by Monte Carlo simulation the morphologies of AB diblock copolymer melts confined in cylindrical tubes selective for one of the blocks, and identified curved lamellae parallel to the tube wall. Performing two-dimensional Monte Carlo simulations for a circle, they identified lamellae parallel to the latter when the surface of the circle was selective for one of the blocks and lamellae in the form of arcs of circles that contacted the wall at their ends with the tendency to become normal to the latter for neutral walls. Sevink et al.,[24] employing the density functional theory (DFT), identified a stacked-disk macrodomain normal to the tube axis for neutral or almost neutral walls, and circular lamellae parallel to the tube surface for strong preferential interactions with one of the

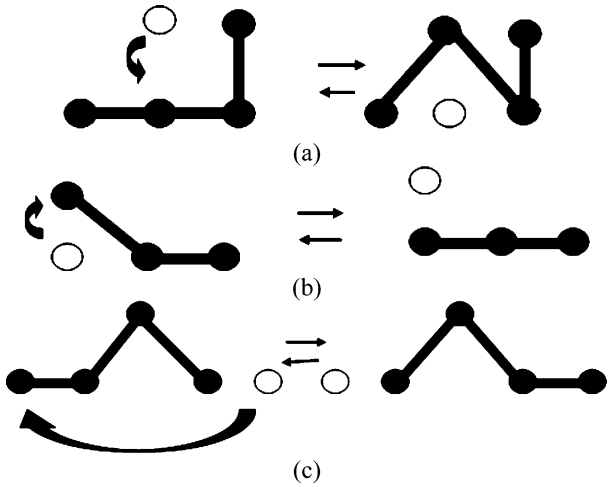

Figure 1. Motions considered in the modified bond-fluctuation and vacancy diffusion Monte Carlo algorithm.

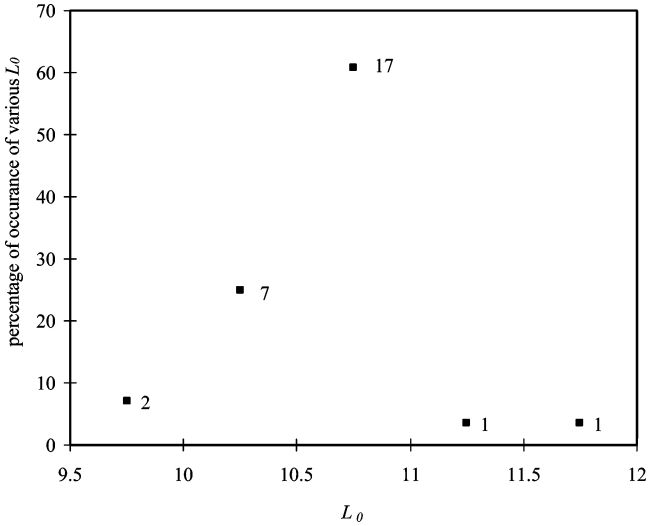

Figure 2. Distribution of the lamellae periods L_0 of AB diblock copolymer melts in the bulk (the number near each of the points in the figure refers to the number of times that value of L_0 occurred in our calculations).

* Corresponding author. Telephone: +1-716-645-2911/ext 2214. Fax: +1-716-645-3822. E-mail address: feaeliru@buffalo.edu.

10.1021/ma0605954 CCC: $33.50
Published on Web 06/08/2006

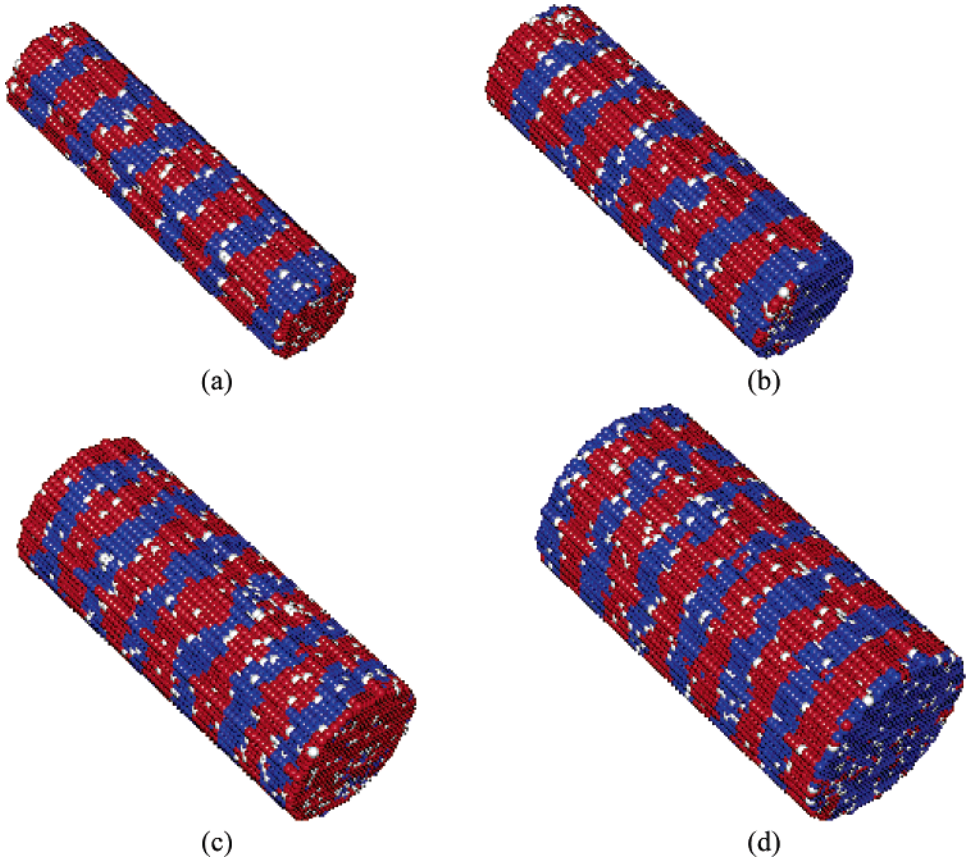

Figure 3. Morphologies of AB diblock copolymer melts confined in cylindrical tubes with lengths of 66× lattice parameter, various diameters, and $\epsilon_{AB} = 0.30k_BT$, $\epsilon_{AV} = \epsilon_{BV} = 0$, $\epsilon_{AA} = \epsilon_{BB} = \epsilon_{VV} = 0$, $\epsilon_{AS} = -0.05k_BT$ and $\epsilon_{BS} = \epsilon_{VS} = 0$. Key: red, A segments; blue, B segments; white, vacancies. (a) $d/L_0 \approx 1.5-1.6$; (b) $d/L_0 \approx 1.9-2.0$; (c) $d/L_0 \approx 2.5-2.6$; (d) $d/L_0 \approx 3.0-3.1$.

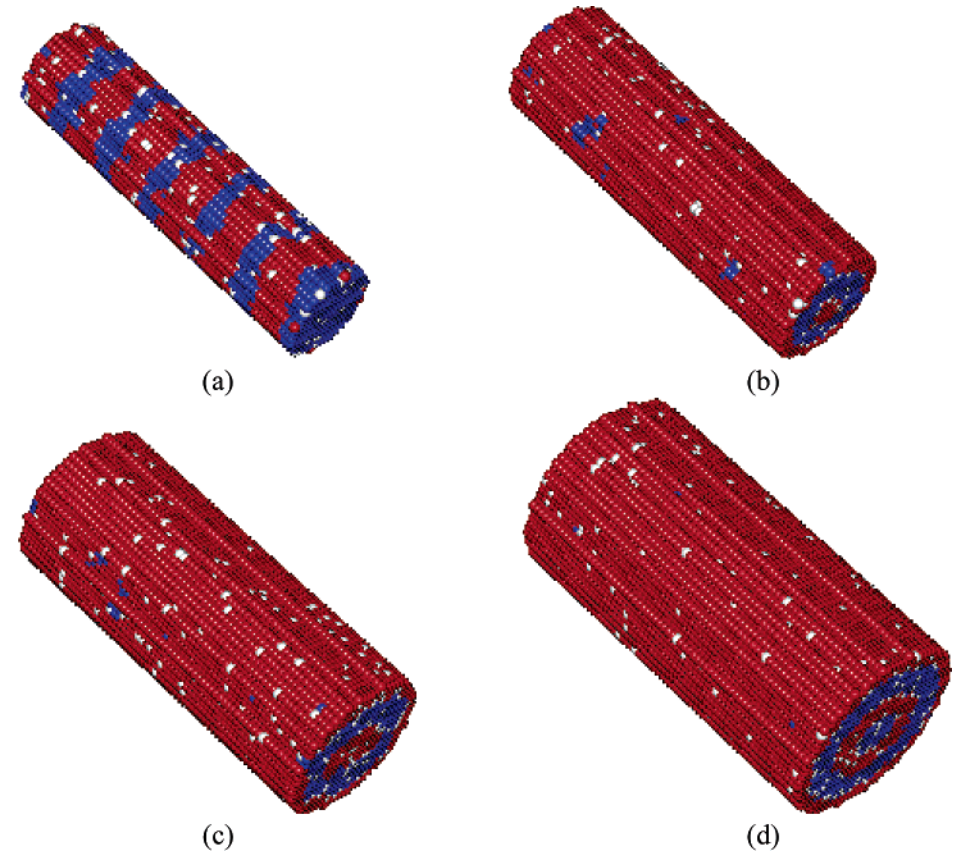

Figure 4. Morphologies of AB diblock copolymer melts confined in cylindrical tubes with length of 66× lattice parameter, various diameters, and $\epsilon_{AB} = 0.30k_BT$, $\epsilon_{AV} = \epsilon_{BV} = 0$, $\epsilon_{AA} = \epsilon_{BB} = \epsilon_{VV} = 0$, $\epsilon_{AS} = -0.11k_BT$, and $\epsilon_{BS} = \epsilon_{VS} = 0$. Key: red, A segments; blue, B segments; white, vacancies. (a) $d/L_0 \approx 1.5-1.6$; (b) $d/L_0 \approx 1.9-2.0$; (c) $d/L_0 \approx 2.5-2.6$; (d) $d/L_0 \approx 3.0-3.1$.

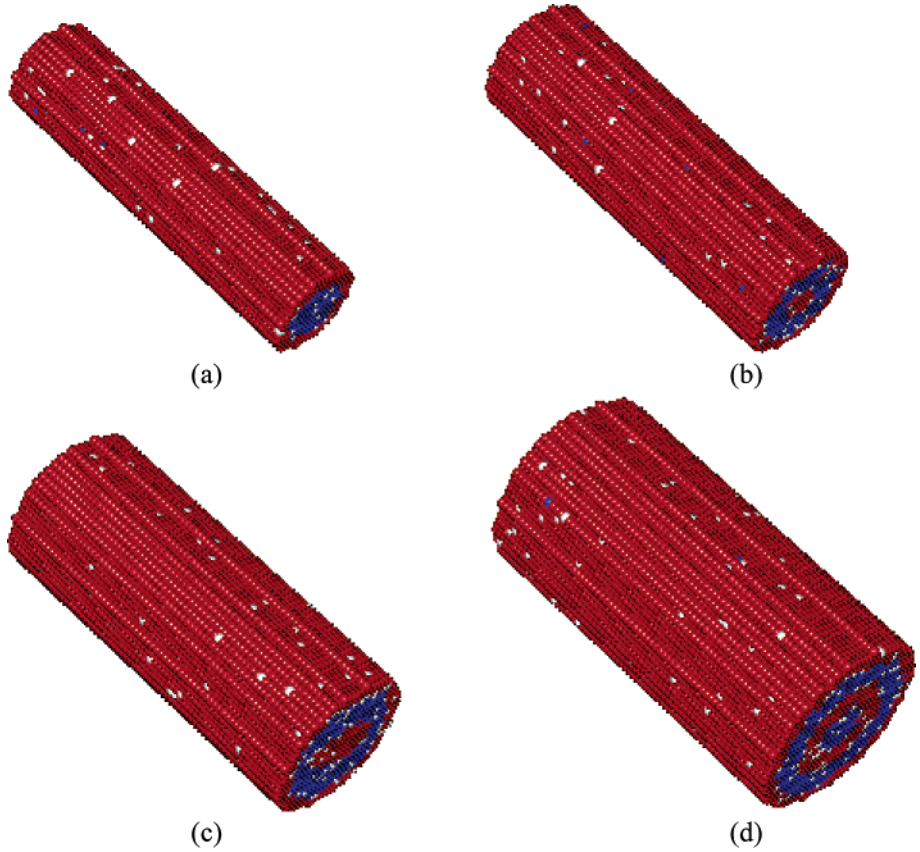

Figure 5. Morphologies of AB diblock copolymer melts confined in cylindrical tubes with length of 66× lattice parameter, various diameters, and $\epsilon_{AB} = 0.30k_BT$, $\epsilon_{AV} = \epsilon_{BV} = 0$, $\epsilon_{AA} = \epsilon_{BB} = \epsilon_{VV} = 0$, $\epsilon_{AS} = -0.30k_BT$, and $\epsilon_{BS} = \epsilon_{VS} = 0$. Key: red, A segments; blue, B segments; white, vacancies. (a) $d/L_0 \approx 1.5-1.6$; (b) $d/L_0 \approx 1.9-2.0$; (c) $d/L_0 \approx 2.5-2.6$; (d) $d/L_0 \approx 3.0-3.1$.

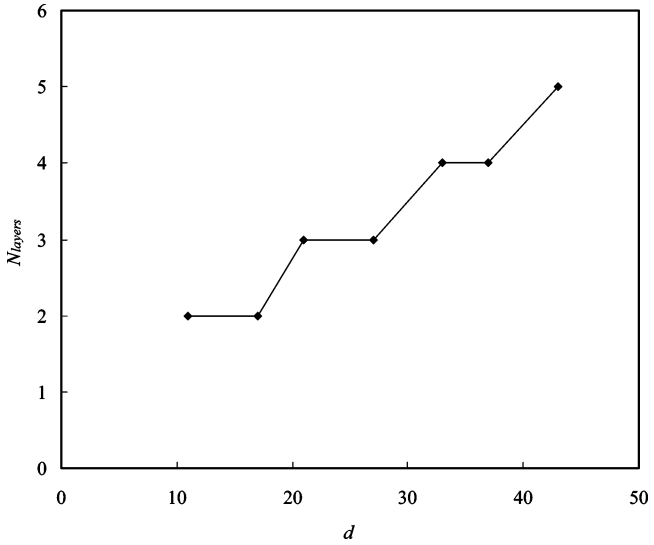

Figure 6. Number of layers in cylindrical tubes with length of 66× lattice parameter, various diameters and $\epsilon_{AB} = 0.30k_BT$, $\epsilon_{AV} = \epsilon_{BV} = 0$, $\epsilon_{AA} = \epsilon_{BB} = \epsilon_{VV} = 0$, $\epsilon_{AS} = -0.30k_BT$, and $\epsilon_{BS} = \epsilon_{VS} = 0$.

blocks. Xiang et al.[25] investigated experimentally the self-assembly of PS/PBD (polystyrene/polybutadiene) diblock copolymers confined in cylindrical nanopores and identified similar structures. Shin et al. found experimentally stacked-disk microdomain normal to the tube axis in highly incommensurate nanotubes, and circular lamellae parallel to the tube surface in commensurate ones.[26] Furthermore, regarding the asymmetrical PS/PBD melts, Xiang et al. found a helical morphology in nanotubes with a diameter d of 33−45 nm ($d/L_0 \sim 1.1-1.5$).[27] They speculated that this helical morphology was generated through the transformation of the hexagonal cylinders formed in tubes with large diameters (e.g., $d \sim 120$ nm and $d/L_0 \sim 4.1$) into helixes, because of the strong confinement by the tubes with small diameters. Wu et al. observed single and double helixes in silica−surfactant composites confined in cylindrical nanochannels by both experiment and self-consistent field calculations.[28] Very recently, Li et al. presented a phase diagram for a diblock copolymer melt under cylindrical confinement.[29] By considering that the structures of AB diblock copolymer melts are translationally invariant along the axis of the cylinder they reduced the problem to a two-dimensional one. However, previous results indicated that some structures will be missed if the three-dimensional case is replaced by the two-dimensional one.

This paper is focused on the morphologies of symmetrical AB diblock copolymer melts confined in nanocylindrical tubes. The effects of the d/L_0 ratio, of the preference of the tube wall for one of the segments and of the interaction between different segments will be investigated by Monte Carlo simulations.

II. Method

A cubic lattice model was employed in the simulations. Because of the high concentrations of the involved segments of the blocks, the algorithms that have been successfully employed for dilute polymer solutions could not be effectively extended to the present case. We adopted a combination[10] between the bond fluctuation model,[30] in which each attempted motion either kept the bond length or changed the bond length from 1× to $\sqrt{2}$× lattice parameter or in the opposite direction, and the volume diffusion algorithm,[31] in which the master of motion was the vacancy. The considered motions are presented in Figure 1. Any attempted motion should obey the excluded

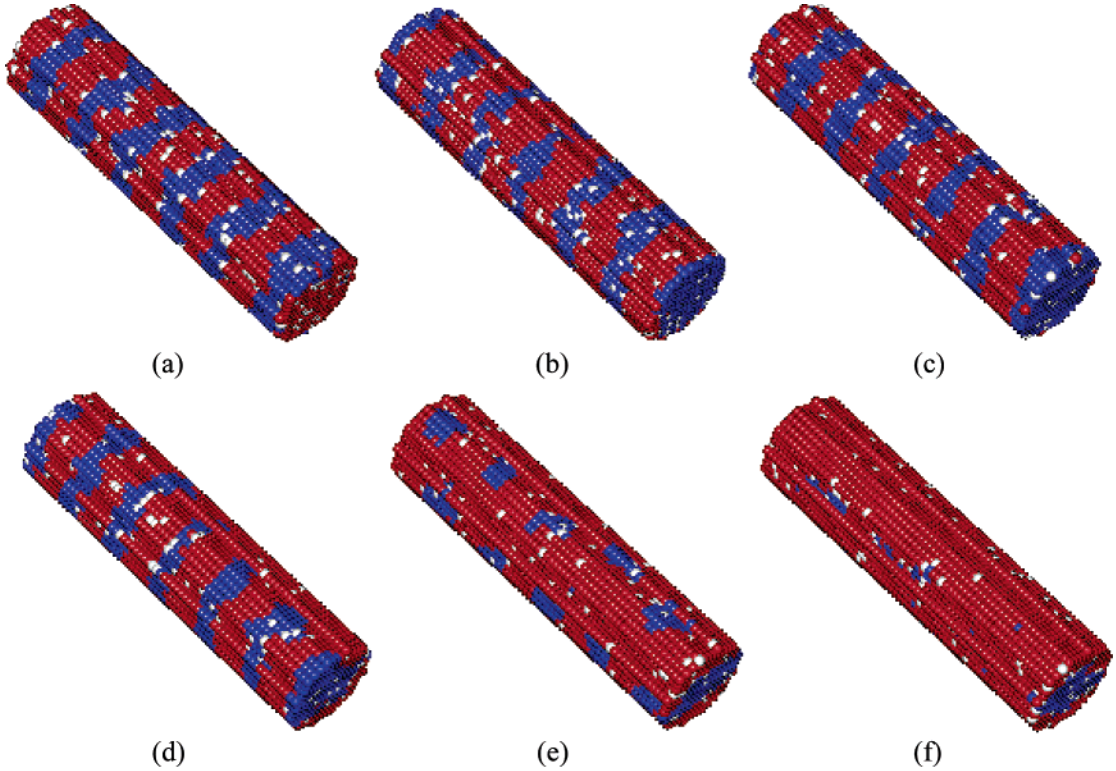

Figure 7. Morphologies of AB diblock copolymer melts confined in cylindrical tubes with length of 66× lattice parameter, various preferences of the surface for segments A, and $\epsilon_{AB} = 0.30k_BT$, $\epsilon_{AV} = \epsilon_{BV} = 0$, $\epsilon_{AA} = \epsilon_{BB} = \epsilon_{VV} = 0$ and $\epsilon_{BS} = \epsilon_{VS} = 0$. Key: red, A segments; blue, B segments; white, vacancies. (a) $\epsilon_{AS} = -0.05k_BT$; (b) $\epsilon_{AS} = -0.10k_BT$; (c) $\epsilon_{AS} = -0.11k_BT$; (d) $\epsilon_{AS} = -0.12k_BT$; (e) $\epsilon_{AS} = -0.14k_BT$; (f) $\epsilon_{AS} = -0.20k_BT$.

volume, no-bond-crossing, and the above bond length restrictions. The traditional Metropolis algorithm was employed to select the acceptance or rejection of any attempted motion.

In this paper, the A_5B_5 (five segments of A and five segments of B) diblock copolymer with a volume fraction of 0.909 was investigated. The remaining volume fraction is occupied by vacancies. In most cases, the length of the cylindrical tube was 66× lattice parameter. To verify that the structures obtained were not artificial consequences of the periodic boundary conditions, tube lengths of 99× lattice parameter were also considered in some cases. To increase the probability that the structures were stable, all the results presented in this paper were obtained after the large number 5×10^7 of Monte Carlo steps.

III. Results and Discussion

A. Lamellae Period L_0 in Bulk for Symmetrical AB Diblock Copolymer Melts. As noted in previous experiments and calculations regarding thin diblock copolymer films, the commensurability between the film thickness h and the characteristic period L_0 in the bulk plays an important role in determining the orientation of the lamellae in films confined between parallel surfaces. Similarly, in a tube, the commensurability between the tube diameter d and the characteristic period L_0 of the bulk determines in a major way the structure of the melt. However, as well-known, the true value of L_0 cannot be obtained easily by Monte Carlo simulations and the matching between the size of the simulation box and the period L_0 of the lamellae is crucial in determining the true value of L_0. Presently, there is no way to obtain the exact value of L_0 by Monte Carlo simulations. As an approximation, Wang et al. performed simulations on bulk systems with various simulation box sizes and calculated L_0 for each case. The value of L_0 with the highest frequency of occurrence was considered as the "true" value (for details one can see ref 8). Following their method, the lamellae period L_0 in the bulk for various simulation box sizes was calculated and the results are presented in Figure 2. To determine L_0, the interaction energies ϵ_{AV}, ϵ_{BV}, ϵ_{AA}, ϵ_{BB}, ϵ_{VV} were taken as zero and ϵ_{AB} was taken as $0.30k_BT$, values which have been employed in most of the simulations in part B. Above, T is the absolute temperature, k_B is the Boltzmann constant, and the subscripts A, B, and V refer to the segments A and B and to vacancies V, respectively. As shown in Figure 2, there is no single value for L_0, and the value of L_0 with the highest frequency is 10.75× lattice parameter. One can therefore estimate the "true" value of L_0 to be approximately in the range of 10.5−11.0× lattice parameter.

B. Morphologies of AB Diblock Copolymer Melts Confined in Cylindrical Tubes. Let us consider that the interaction between the two segments A and B $\epsilon_{AB} = 0.30k_BT$ and that the interactions between the polymer segments and the vacancies $\epsilon_{AV} = \epsilon_{BV} = 0$. In addition, the interactions between the same species are taken $\epsilon_{AA} = \epsilon_{BB} = \epsilon_{VV} = 0$. For the weak selectivity of the surface of the tube for the A segments $\epsilon_{AS} = -0.05k_BT$ and $\epsilon_{BS} = \epsilon_{VS} = 0$ (Figure 3), where the subscript S refers to the surface of the tube, the symmetric AB diblock copolymer melts form separate lamellae of A and B normal to the tube axis in both the commensurate and incommensurate cases. These results are in agreement with the density functional theory (DFT) calculations of Sevink et al.[26] This occurs because the interactions between the segments and the surface are weak (even zero for B) and the interaction between A and B is strongly repulsive. By changing the strength of the selectivity of the tube surface for the A segments to $\epsilon_{AS} = -0.11k_BT$, circular lamellae parallel to the tube surface have been observed in the commensurate cases $d/L_0 \approx 1.9-2.0$ and $d/L_0 \approx 3.0-3.1$ (Figure 4, parts b and d), and normal lamellae were identified for $d/L_0 \approx 1.5-1.6$ (Figure 4a). Circular lamellae are formed in the former case as a result of the sufficiently strong interactions between the A

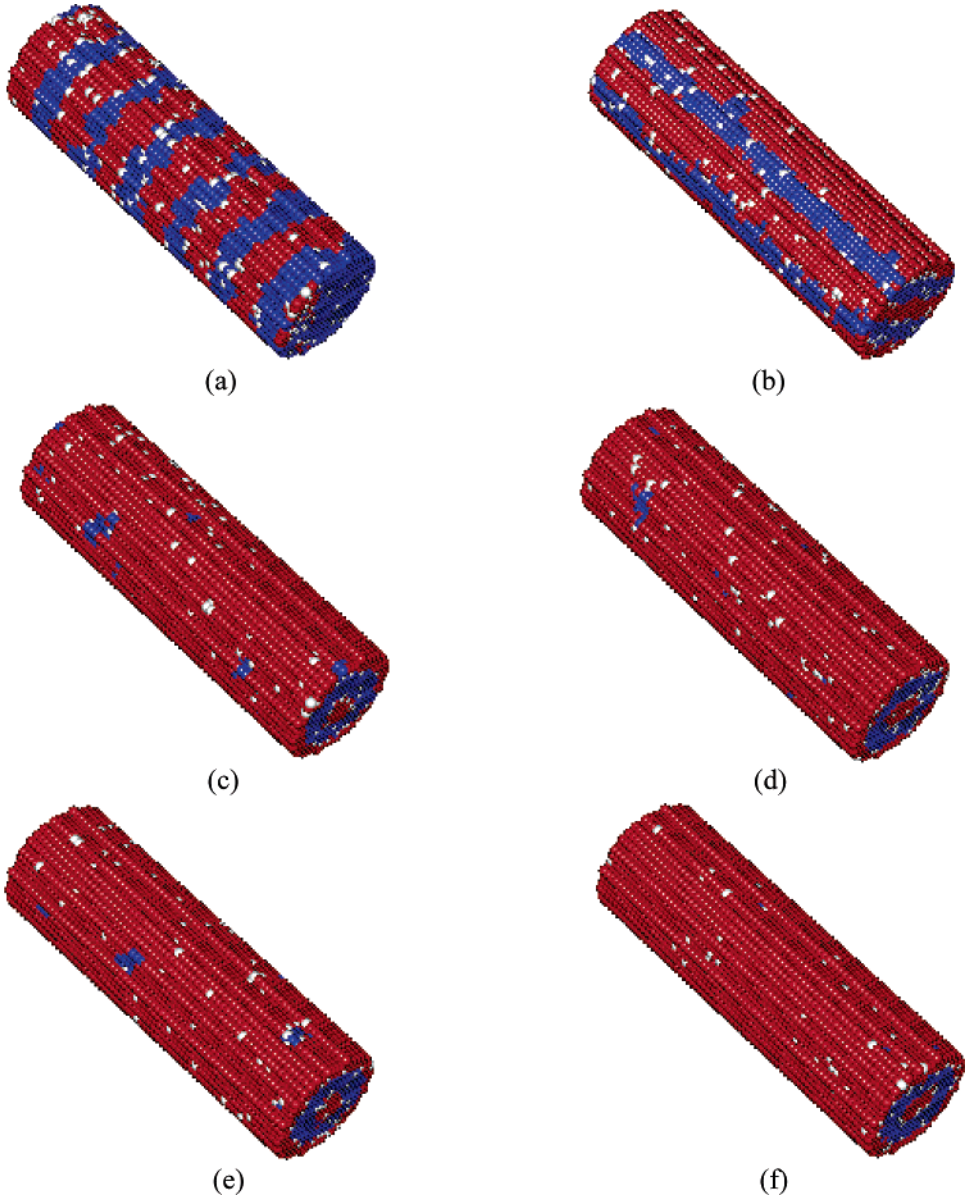

Figure 8. Morphologies of AB diblock copolymer melts confined in cylindrical tubes with length of 66× lattice parameter, various preferences of the surface for the A segments, and $\epsilon_{AB} = 0.30k_BT$, $\epsilon_{AV} = \epsilon_{BV} = 0$, $\epsilon_{AA} = \epsilon_{BB} = \epsilon_{VV} = 0$ and $\epsilon_{BS} = \epsilon_{VS} = 0$. Key: red, A segments; blue, B segments; white, vacancies. (a) $\epsilon_{AS} = -0.05k_BT$; (b) $\epsilon_{AS} = -0.10k_BT$; (c) $\epsilon_{AS} = -0.11k_BT$; (d) $\epsilon_{AS} = -0.12k_BT$; (e) $\epsilon_{AS} = -0.14k_BT$; (f) $\epsilon_{AS} = -0.20k_BT$.

Table 1. Structures of A_5B_5 Diblock Copolymer Melts Confined in Nanocylindrical Tubes for Various Ratios of Diameter to Lamellae Period (d/L_0) and Various Surface preferences (ϵ_{AS}) under the Conditions $\epsilon_{AV} = \epsilon_{BV} = \epsilon_{AA} = \epsilon_{BB} = \epsilon_{VV} = \epsilon_{BS} = \epsilon_{VS} = 0$ and $\epsilon_{AB} = 0.30k_BT$

	d/L_0			
ϵ_{AS}	1.5−1.6	1.9−2.0	2.5−2.6	3.0−3.1
$-0.05k_BT$	lamellae normal to the tube axis	lamellae normal to the tube axis	lamellae normal to the tube axis	lamellae normal to the tube axis
$-0.10k_BT$	lamellae normal to the tube axis	lamellae parallel to the tube axis		
$-0.11k_BT$	lamellae normal to the tube axis	circular lamellae	circular lamellae	circular lamellae
$-0.12k_BT$	lamellae normal to the tube axis (some connection between lamellae)	circular lamellae		
$-0.14k_BT$	mesh structure	circular lamellae		
$-0.20k_BT$	circular lamellae	circular lamellae		
$-0.30k_BT$	circular lamellae	circular lamellae	circular lamellae	circular lamellae

segments and the surface. In the latter case, normal lamellae are formed probably because the incommensurability between the diameter d and the lamellae period in the bulk L_0 plays a more important role than the interaction energy of the tube surface with the A segments. It is notable that circular lamellae parallel to the tube surface are also present in the incommensurate case $d/L_0 \approx 2.5-2.6$ (Figure 4c). This probably occurs because the frustration of the lamellae thickness in the

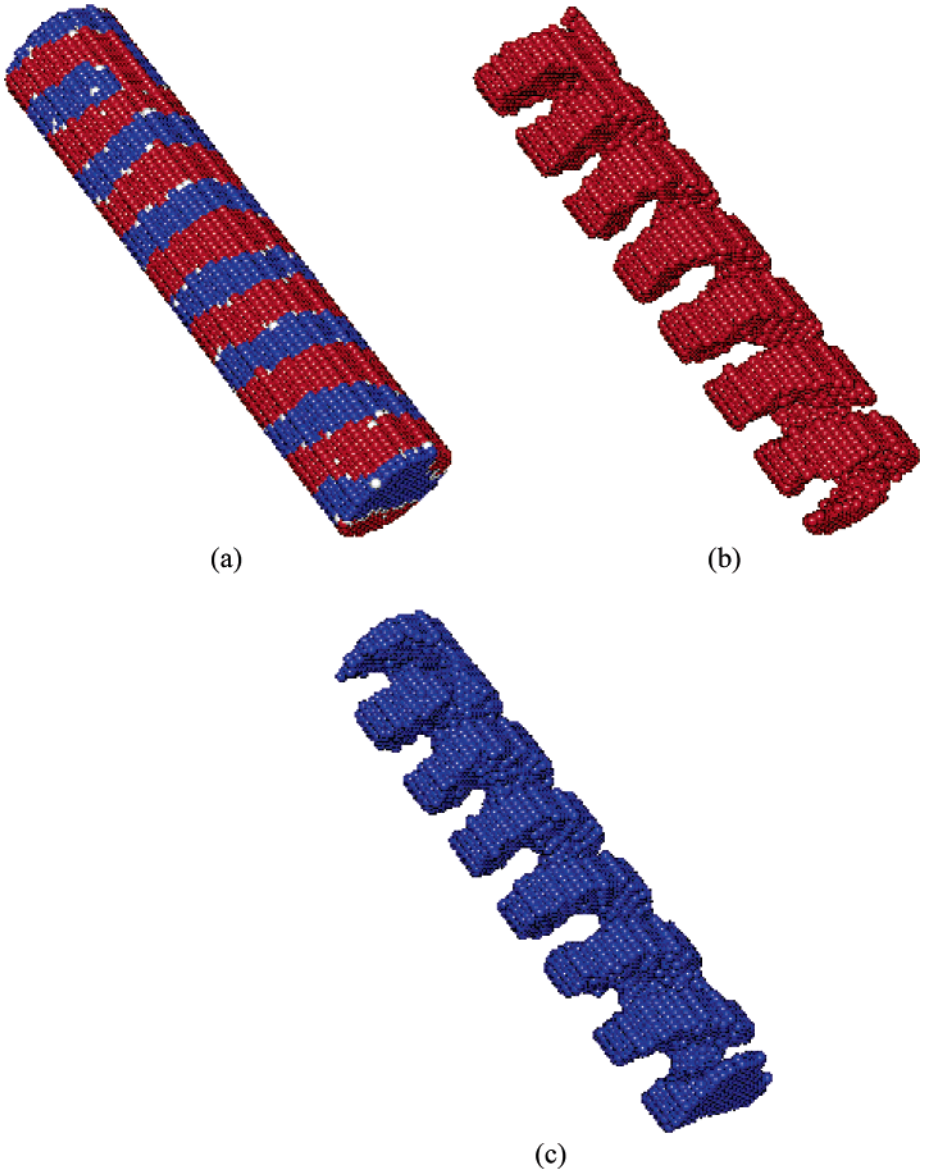

Figure 9. Single helix structure in AB diblock copolymer melts confined in cylindrical tubes with length of 99× lattice parameter, $d/L_0 \approx 1.9-2.0$, and $\epsilon_{AB} = 1.10k_BT$, $\epsilon_{AV} = \epsilon_{BV} = 0$, $\epsilon_{AA} = \epsilon_{BB} = \epsilon_{VV} = 0$, $\epsilon_{AS} = -0.09k_BT$ and $\epsilon_{BS} = \epsilon_{VS} = 0$. Key: red, A segments; blue, B segments; white, vacancies. (a) Full image is shown. (b) The image contains only the A segments. (c) The image contains only the B segments.

tube is, in this case, nearer to that of a commensurate one than when $d/L_0 \approx 1.5-1.6$ (Figure 4a). When ϵ_{AS} is further changed to $-0.30k_BT$ (Figure 5), circular lamellae parallel to the tube surface are formed because the preferential interaction of the tube surface with the A segments overcomes the effect of the incommensuration between the diameter and the period of the lamellae in the bulk. Figure 6 presents the relationship between the number of layers with lamellar structures parallel to the tube surface and the diameter of the tube, and shows that the same number of layers occurs for the tubes with $d/L_0 = n + (1/2)$ as for the tubes with $d/L_0 = n$, where n is an integer.

The above results show that the competition between the incommensurability of d and L_0 and the preference of the tube surface for the A segments plays a role when (*i*) the diameter of the tube becomes comparable with the lamellae period L_0 ($1.5-2.0\ L_0$) and (ii) the preference of the surface for the A segments is neither too strong nor too weak. When it is too strong, circular lamellae are formed regardless of the value of the ratio d/L_0. When it is too weak, normal lamellae are generated. The mentioned competition can induce some interesting morphologies in diblock copolymer melts confined in nanotubes. In Figure 7, the morphologies of the symmetrical AB diblock copolymer melts confined in incommensurate tubes with $d/L_0 \approx 1.5-1.6$ ($d = 17\times$ lattice parameter) are presented by varying ϵ_{AS} from $-0.05k_BT$ to $-0.20k_BT$. As noted previously, when $|\epsilon_{AS}|$ was smaller than $0.11k_BT$, lamellae normal to the tube axis were observed (Figure 7a−c). By increasing $|\epsilon_{AS}|$ to $0.12k_BT$, some connections between the A segments of the lamellae appeared (Figure 7d), and by increasing $|\epsilon_{AS}|$ to $0.14k_BT$, the normal lamellae became circular, parallel to the tube surface, and contained pores (mesh phases) (Figure 7e). Finally, by further increasing $|\epsilon_{AS}|$ to $0.20k_BT$, the sites on the tube surface became mostly occupied by the A segments and the mesh lamellae parallel to the tube surface were replaced by circular lamellae parallel to the tube surface, because of the higher preference of the surface for the A segments (Figure 7f). For comparison, commensurate cases with a diameter of $d = 21\times$ lattice parameter ($d/L_0 \approx 1.9-2.0$) have been also simulated. As noted before, lamellae normal to the tube axis were formed when the preference of the surface for the A segments was weak ($\epsilon_{AS} = -0.05k_BT$) (Figure 8a). Lamellae parallel to the tube axis rather than lamellae normal to the tube

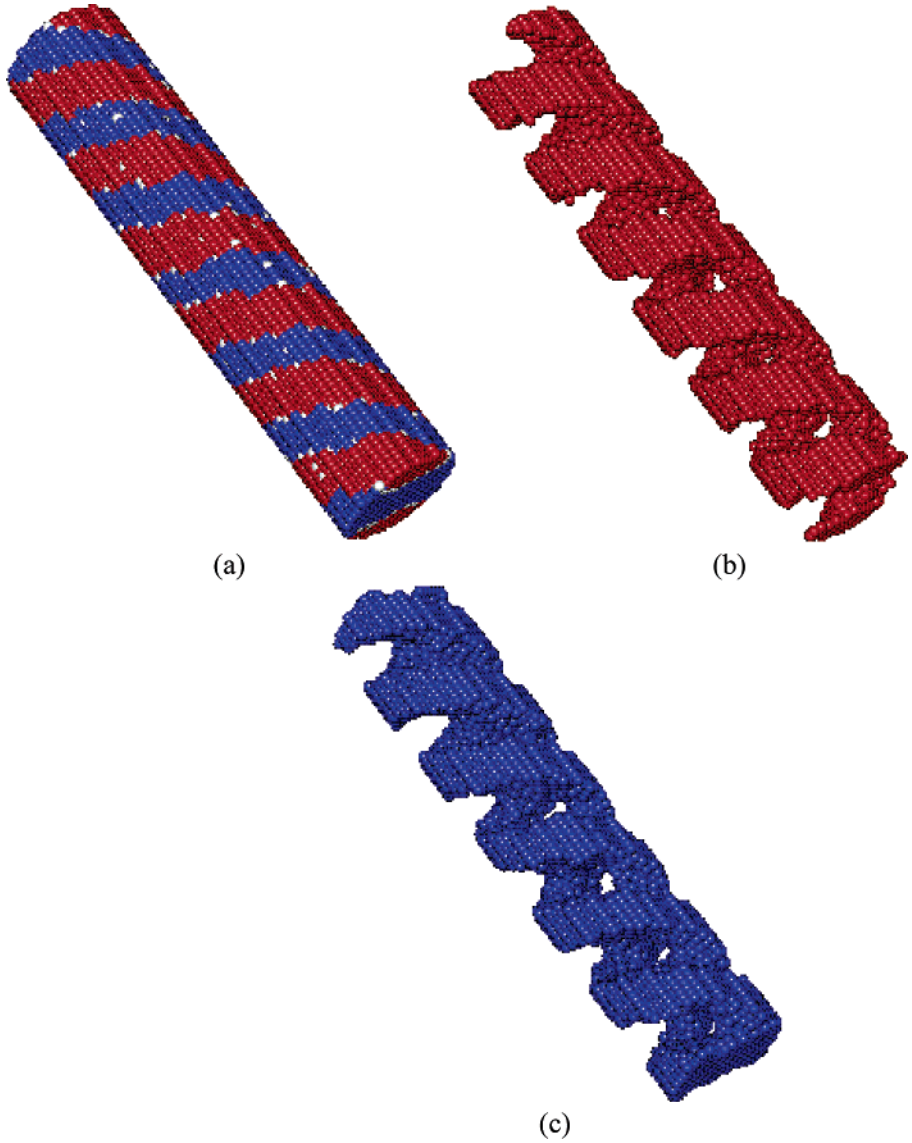

Figure 10. Double helix structure in AB diblock copolymer melts confined in cylindrical tubes with length of 99× lattice parameter, $d/L_0 \approx 1.9-2.0$, and $\epsilon_{AB} = k_BT$, $\epsilon_{AV} = \epsilon_{BV} = 0$, $\epsilon_{AA} = \epsilon_{BB} = \epsilon_{VV} = 0$, $\epsilon_{AS} = -0.10k_BT$ and $\epsilon_{BS} = \epsilon_{VS} = 0$. Key: red, A segments; blue, B segments; white, vacancies. (a) Full image is shown. (b) The image contains only the A segments. (c) The image contains only the B segments.

axis have been observed when ϵ_{AS} became $-0.10k_BT$ (Figure 8b). By changing ϵ_{AS} to $-0.11k_BT$ (which could not change the morphology of the melt from normal lamellae to circular ones in the incommensurate case $d/L_0 \approx 1.5-1.6$), circular lamellae parallel to the tube surface could be identified in the commensurate case $d/L_0 \approx 1.9-2.0$ (Figure 8c). The structure in Figure 8b can be considered an intermediate stage between the structures represented by Figure 8, parts a and c. By increasing $|\epsilon_{AS}|$ further, circular lamellae parallel to the tube surface continued to form (Figure 8d−f). In Table 1, a summary of the structures obtained under various conditions is provided.

Xiang et al.[29] investigated the diblock copolymers of PS-(styrene)-*b*-PBD(butadiene), in which the blocks PS and PBD were highly immiscible. In their experiments, the volume fraction of PBD was 0.36. It is notable that the morphology of PS(styrene)-*b*-PBD(butadiene) melts confined in a tube acquired a helix structure when the diameter of the tube became comparable to the lamellae period L_0. In our simulations, symmetrical AB diblock copolymer melts with high immiscibility between the segments A and B were considered. As shown in Figure 9, a helix consisting of A segments coupled with another helix of B segments were obtained in cylindrical tubes with $d = 21\times$ lattice parameter for $\epsilon_{AB} = 1.10k_BT$ and $\epsilon_{AS} = -0.09k_BT$ (the other interaction energies being the same as before, zero). The formation of the two separated helixes of the A and B segments can be attributed to the following: (i) the relatively strong repulsion between the A and B segments which prevents the occurrence of lamellae normal to the tube axis; (ii) the attractive interaction energy between the tube surface and the A segments is not high enough to generate circular lamellae. Double helixes consisting of A segments coupled with double helixes consisting of B segments have been also observed for $\epsilon_{AB} = k_BT$ and $\epsilon_{AS} = -0.10k_BT$ (Figure 10). The single and double helixes have been first observed for tubes with a length of 66× lattice parameter. The same results were, however, obtained for tubes with a length of 99× lattice parameter. This indicated that the periodic boundary conditions have not induced artificial structures. The helixes represent structures intermediary between the normal and parallel lamellae. The normal situation occurs when the selectivity of the surface for one of the segments is relatively weak, whereas the other occurs when the selectivity is strong. An intermediate selectivity is required for helixes to be formed. The structure containing lamellae parallel to the tube axis (Figure 8b) represents one of

the steps in the transition from the normal lamellae to the surface to parallel lamellae with the surface.

After this work was completed, a paper was published by Chen et al.,[32] which considered the same kind of systems. Lamellae normal to the tube axis and mesh morphologies as well as single helixes were found by them. However, lamellae parallel to the tube axis and double helixes were additionally identified in our work.

IV. Conclusion

In this paper, the morphologies of symmetrical AB diblock copolymer melts confined in cylindrical tubes have been investigated by Monte Carlo simulations. Lamellae normal to the tube axis have been observed in tubes of any diameter for weak preferences of its surface for the A segments. By increasing somewhat the preference for the A segments, the simulations have shown that the competition between the incommensurability of the diameter of the tube d and the lamellae period in the bulk L_0 and the preference of the surface for the A segments became important for comparable values of d and L_0. Furthermore, the incommensurability has driven the transformation of the morphology from circular lamellae, which occur in the commensurate case for the same interaction energy, to lamellae normal to the tube axis. High preferences for the A segments led to circular lamellae in both the commensurate and incommensurate cases. All the above results are consistent with the previous experiments and theoretical calculations. Additionally, we found mesh morphologies and lamellae parallel to the tube axis in tubes with $d/L_0 \approx 1.5-1.6$ ($d = 17\times$ lattice parameter) and $d/L_0 \approx 1.9-2.0$ ($d = 21\times$ lattice parameter), respectively. Single and double helixes were also identified when the two kinds of segments were highly repulsive and preference of the surface for one of the segments was moderate.

References and Notes

(1) Park, M.; Harrison, C.; Chainkin, P. M.; Register, R. A.; Adamson, D. H.; *Science* **1997**, *276*, 1401.
(2) Krausch, G.; Magerle, R. *Adv. Mater.* **2002**, *14*, 1579.
(3) Fredrickson, G. H.; Helfand, E. *J. Chem. Phys.* **1987**, *87*, 697.
(4) Hajduk, D. A.; Takenouchi, H.; Hillmyer, M. A.; Bates, F. S.; Vigild, M. E.; Almdal, K. *Macromolecules* **1997**, *30*, 3788.
(5) Lambooy, P.; Russell, T. P.; Kellogg, G. J.; Mayes, A. M.; Gallagher, P. D.; Satija, S. K. *Phys. Rev. Lett.* **1994**, *72*, 2899.
(6) Kellogg, G. J.; Walton, D. G.; Mayes, A. M.; Lambooy, P.; Russell, T. P.; Gallagher, P. D.; Satija, S. K. *Phys. Rev. Lett.* **1996**, *76*, 2503.
(7) Geisinger, T.; Müller, M.; Binder, K. *J. Chem. Phys.* **1999**, *111*, 5241.
(8) Wang, Q.; Yan, Q. L.; Neeley, P. F.; de Pablo, J. J. *J. Chem. Phys.* **2000**, *112*, 450.
(9) Matsen, M. W.; Thompson, R. B. *J. Chem. Phys.* **1999**, *111*, 7139.
(10) Feng, J.; Ruckenstein, E. *Macromol. Theory Simul.* **2002**, *11*, 630.
(11) Feng, J.; Ruckenstein, E. *Polymer* **2002**, *43*, 5775.
(12) Chen, H.; Chakrabarti, A. *J. Chem. Phys.* **1998**, *108*, 6897.
(13) Wang, Q.; Nath, S. K.; Graham, M. D.; Nealey, P. F.; de Pablo, J. J. *J. Chem. Phys.* **2000**, *112*, 9996.
(14) Williams, D. R. M.; Mackintosh, F. C. *Macromolecules* **1994**, *27*, 7677.
(15) Kodama, H.; Doi, M. *Macromolecules* **1996**, *29*, 2652.
(16) Ren, S. R.; Hamley, I. W. *Phys. Rev. E.* **2001**, *63*, 041503−1.
(17) Ohta, T.; Enomoto, Y.; Harden, J. L.; Doi, M. *Macromolecules* **1993**, *26*, 4928.
(18) Thurn-Albrecht, T.; DeRouchey, J.; Russell, T.; Kolb, R. *Macromolecules* **2002**, *35*, 8106.
(19) Böker, A.; Elbs, H.; Hänsel, H.; Knoll, A.; Ludwigs, S.; Zettl, H.; Urban, V.; Abetz, V.; Müller, A. H. E.; Krausch, G. *Phys. Rev. Lett.* **2002**, *23*, 135502−1.
(20) Kyrylyuk, A. V.; Zvelindovsky, A. V.; Sevink, G. J. A.; Fraaije, J. G. E. M. *Macromolecules* **2002**, *35*, 1473.
(21) Xu, T.; Goldbach, J. T.; Russell, T. P. *Macromolecules* **2003**, *36*, 7296.
(22) Feng, J.; Ruckenstein, E. *J. Chem. Phys.* **2004**, *121*, 1609.
(23) He, X.; Song, M.; Liang, H.; Pan, C. *J. Chem. Phys.* **2001**, *114*, 10510.
(24) Sevink, G. J. A.; Zvelindovsky, A. V.; Fraaije, J. G. E. M.; Huinink, H. P. *J. Chem. Phys.* **2001**, *115*, 8226.
(25) Xiang, H.; Shin, K.; Kim, T.; Moon, S. I.; McCarthy, T. J.; Russell, T. P. *Macromolecules* **2004**, *37*, 5660.
(26) Shin, K.; Xiang, H.; Kim, T.; Moon, S. I.; McCarthy, T. J.; Russell, T. P. *Science* **2004**, *306*, 76.
(27) Xiang, H.; Shin, K.; Kim, T.; Moon, S. I.; McCarthy, T. J.; Russell, T. P. *Macromolecules* **2005**, *38*, 1055.
(28) Wu, Y.; Cheng, G.; Katsov, K.; Sides, S. W.; Wang, J.; Tang, J.; Fredrickson, G. H.; Moskovits, M.; Stucky, G. D. *Nat. Mater.* **2004**, *3*, 816.
(29) Li, W.; Wickham, R. A.; Garbary, R. A. *Macromolecules* **2006**, *39*, 806.
(30) Larson, R. G.; Scriven, L. E.; Davis, T. *J. Chem. Phys.* **1985**, *83*, 2411.
(31) Reiter, J.; Edling, T.; Pakula, T. *J. Chem. Phys.* **1990**, *93*, 837.
(32) Chen, P.; He, X.; Liang, H. *J. Chem. Phys.* **2006**, *124*, 104906.

MA0605954